Letter

Nonlocality of Majorana bound states revealed by electron waiting times in a topological Andreev interferometer

Paramita Dutta [1], Jorge Cayao [2], Annica M. Black-Schaffer [2], and Pablo Burset [3]

[1] *Theoretical Physics Division, Physical Research Laboratory, Ahmedabad 380009, India*

[2] *Department of Physics and Astronomy, Uppsala University, Box 516, S-751 20 Uppsala, Sweden*

[3] *Department of Theoretical Condensed Matter Physics, Condensed Matter Physics Center (IFIMAC) and Instituto Nicolás Cabrera, Universidad Autónoma de Madrid, 28049 Madrid, Spain*

(Received 4 July 2023; revised 24 November 2023; accepted 15 January 2024; published 19 March 2024)

The analysis of waiting times of electron transfers has recently become experimentally accessible owing to advances in noninvasive probes working in the short-time regime. We study electron waiting times in a topological Andreev interferometer: a superconducting loop with controllable phase difference connected to a quantum spin Hall edge, where the edge state helicity enables the transfer of electrons and holes into separate leads, with transmission controlled by the loop's phase difference ϕ. This setup features gapless Majorana bound states at $\phi = \pi$. The waiting times for electron transfers across the junction are sensitive to the presence of the gapless states, but are uncorrelated for all ϕ. By contrast, at $\phi = \pi$ the waiting times of Andreev-scattered holes show a strong correlation and the crossed (hole-electron) distributions feature a unique behavior. Both effects exclusively result from the nonlocal properties of Majorana bound states. Consequently, electron waiting times and their correlations could circumvent some of the challenges for detecting topological superconductivity and Majorana states beyond conductance signatures.

DOI: 10.1103/PhysRevResearch.6.L012062

Introduction. Fluctuations in electron transport can greatly impact the performance of electronic circuits but, at the same time, provide us with invaluable information about the quantum-coherent behavior of conductors [1]. Charge fluctuations are often analyzed by full counting statistics [2–4], which usually concerns the zero-frequency or long-time limit. However, experimental advances with noninvasive probes [5–7] have now enabled access to the short-time regime with almost single-event resolution.

A prominent, recently developed tool for the short-time regime is the electron waiting time distribution (WTD): the distribution of time intervals between consecutive charge transfers. Electron WTDs provide information about tunneling events in mesoscopic conductors beyond average current and noise [8–17], and have recently been measured in quantum dots connected to metallic electrodes [6,18–20] and superconductors [21,22]. Moreover, correlations between waiting times indicate nonrenewal quantum transport [16], where electron transfers are not independent or identically distributed, making WTDs a source of information distinct from other statistical tools [14,16,17].

In this Letter, we analyze the potential of electron WTDs and their correlations for identifying topological superconductors hosting Majorana bound states (MBSs) [23–26]. There is currently an intense research activity focused on obtaining reliable signatures of MBSs, since the simplest one, a robust and quantized zero-bias conductance peak [27–29], has proven insufficient [30,31]. Electron waiting times in superconducting hybrid junctions have already been proposed to characterize the entanglement between the electrons in Cooper pairs [32–34] and to detect the presence of MBSs [35–39]. These

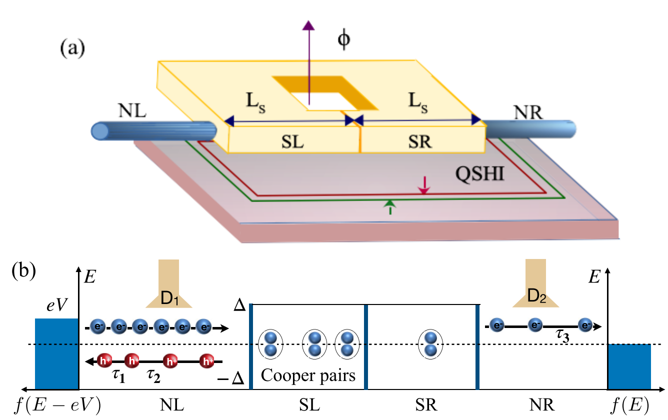

FIG. 1. (a) Andreev interferometer at the QSHI edge with magnetic flux ϕ applied through a superconductor loop. (b) Incident electrons (blue balls) with energy within the gap Δ scatter off the NL-SL-SR-NR junction only as electron transmissions to NR or Andreev-reflected holes (red balls) into NL. Detectors D_1 and D_2, respectively, placed at NL and NR, detect electrons or holes either individually or simultaneously. NL is biased by a voltage V and NR is at equilibrium.

theoretical proposals extended the concept of waiting times to both spin and electron-hole degrees of freedom, but they have still primarily only focused on the *local* properties of MBSs [35–39]. Instead, we here suggest a Majorana platform without magnetic materials that is both conceptually simple and presents important advantages for measuring waiting times of electrons and holes and their *nonlocal* properties: an Andreev interferometer built on the edge of a quantum spin Hall insulator (QSHI) [40–46] [Fig. 1(a)].

The QSHI features helical edge states consisting of one-dimensional Dirac fermions characterized by spin-momentum locking [47,48]. When proximitized by a narrow superconducting lead [49–56], the helical edge states guarantee that only electrons tunnel through the lead and only Andreev-converted holes are reflected [57–66]. Consequently, the superconductor acts as a beam splitter that separates electrons from holes into different leads and allows independent detection, see Fig. 1(b). In the interferometer setup [67,68], a superconducting loop with controllable phase difference ϕ is connected to the QSHI edge [Fig. 1(a)], so that the electric conductance at the NL or NR sides depends periodically on ϕ. Importantly, recent experiments [51–53] have found that the lowest-energy bound states formed at the SL-SR interface are always gapless at $\phi = \pi$, and thus MBSs [24,25].

Due to the lack of a gap, the topological MBSs dominate the local and nonlocal transport across the interferometer. We find that the waiting times for electron transfers across our junction are sensitive to the MBSs, but are uncorrelated with each other. By contrast, the waiting times of Andreev reflected holes are less sensitive to the MBSs, but instead present a strong correlation at $\phi \sim \pi$. Importantly, the crossed (hole-electron) distributions and their correlations feature a unique behavior characteristic of a gapless nonlocal MBS. Consequently, electron waiting times and their correlations constitute an alternative signature of MBSs, sensitive to their nonlocal nature, thus circumventing the problems arising from trivial resonant levels that naturally form in many Majorana platforms [30].

Topological Andreev interferometer. We consider an Andreev interferometer at the edge of a QSHI (Fig. 1), which comprises of a superconducting loop with a short SL-SR junction that is attached to the normal metal leads NL and NR. For simplicity, we fix the length of each superconductor segment to be equal, L_S, and only analyze the situation where SL and SR share an interface [Fig. 1(b)] [69]. Low-energy excitations are described in the basis $\Psi(x) = (\psi_\uparrow, \psi_\downarrow, \psi_\downarrow^\dagger, -\psi_\uparrow^\dagger)^T$, with $\psi_\sigma^\dagger(x)$ the creation operator for electrons with spin $\sigma \in \{\uparrow, \downarrow\}$ at position x, by the Bogoliubov-de Gennes Hamiltonian [62]

$$H_{\mathrm{BdG}} = \hbar v_F k_x \hat{\eta}_3 \hat{\sigma}_3 - \mu \hat{\eta}_3 \hat{\sigma}_0 + \Delta(x) \hat{\eta}_1 \hat{\sigma}_0. \quad (1)$$

Here, v_F is the Fermi velocity, μ the chemical potential, and the Pauli matrices $\hat{\eta}_j$ and $\hat{\sigma}_j$ act in Nambu and spin spaces, respectively. We set the pair potential $\Delta(x) = \Delta$ for SL, $\Delta(x) = \Delta e^{i\phi}$ for SR (ϕ is the superconducting phase difference), and zero otherwise. Henceforth, we set $v_F = \hbar = \Delta = 1$ so that the superconducting coherence length is $\xi = \hbar v_F/\Delta = 1$ [70] and set $\mu = 0$ and $eV = \Delta/2$ [71], see Supplemental Material (SM) [72]. The QSHI Andreev interferometer forms a topological Josephson-like junction that hosts gapless MBSs at the SL-SR interface at $\phi = \pi$ [25,65]. For any other trivial junction, the bound states develop a gap around $\phi \sim \pi$. To distinguish between topological (gapless) and trivial (gapful) bound states, we compare below the prototypical cases $\phi = 0$ and $\phi = \pi$. Although our junction is always topological, results at $\phi = 0$ are qualitatively equivalent to those of a trivial bound state (for any ϕ), as long as its gap is comparable or larger than the bias eV.

Electron waiting times. WTDs for phase-coherent transport of noninteracting electrons are evaluated from the scattering matrix [9,10,36]. Generally an Andreev interferometer has four effective transport channels [electrons or holes (e, h), incoming or outgoing (i, o), from the left or right leads (L, R)], represented by the spinor $\Psi^{i(o)} = (\psi_{eL}^{i,(o)}, \psi_{hL}^{i(o)}, \psi_{eR}^{i(o)}, \psi_{hR}^{i(o)})^T$. For a given energy E, the scattering matrix connects outgoing and incoming solutions of Eq. (1) as $\Psi^{(o)} = \mathcal{S}\Psi^{(i)}$ (see the SM [72]). Owing to the spin-momentum locking at the QSHI edge, here only the normal transmissions $\mathcal{S}_{\alpha L,\alpha R}$ and $\mathcal{S}_{\alpha R,\alpha L}$, with $\alpha = e, h$, and the Andreev reflections $\mathcal{S}_{eX,hX}$ and $\mathcal{S}_{hX,eX}$, with $X = L, R$, are nonzero. From the scattering matrix we define the idle-time probability $\Pi(\{\tau_\gamma\})$ that no particles of type $\gamma = \alpha X$ are detected during the time interval τ_γ (for the stationary processes considered here only time intervals are relevant). Following Refs. [10,36], we have

$$\Pi(\{\tau_\gamma\}) = \det[\mathcal{I} - \mathcal{S}^\dagger(E)\mathcal{K}(\{\tau_\gamma\}, E - E')\mathcal{S}(E')], \quad (2)$$

where $\mathcal{I}$ is the identity matrix and $\mathcal{K}$ is a diagonal matrix, $\mathcal{K}(\{\tau_\gamma\}, E) = \bigoplus_\gamma K(\tau_\gamma, E)$, with the kernels (see the SM [72])

$$K(\tau_\gamma, E) = \kappa e^{-iE\tau_\gamma/2} \sin(E\tau_\gamma/2)/(\pi E). \quad (3)$$

The linear dispersion relation of the QSHI helical edge states allows us to naturally divide the transport window $[\mu, \mu + eV]$ in intervals of width $\kappa = eV/N$, where N is the total number of intervals and eV the applied bias. Due to the inversion symmetry of our setup, we only consider voltages applied to the left lead, $V_L \equiv V$, $V_R = 0$. We work in the limit $N \to \infty$ where Eq. (3) correctly applies to stationary transport [10].

We can now define $\mathcal{W}_{\alpha\beta}(\tau) = -\langle\tau_\alpha\rangle\partial_\tau^2\Pi(\tau)$ as the probability density of detecting a particle of type β at a time τ after having measured a particle of type α (see the SM [72]). Here, the mean waiting time $\langle\tau_\alpha\rangle$ is related to the average current for α particles, $I_\alpha = 1/\langle\tau_\alpha\rangle$. Analogously, we define the joint waiting time $\mathcal{W}_{\alpha\gamma\beta}(\tau_1, \tau_2) = \langle\tau_\alpha\rangle\partial_{\tau_1}\partial_{\tau_2}^2\Pi$, which generalizes the waiting time distribution between particles of type α and β to include the extra detection of a particle of type γ at an intermediate time τ_1, such that $0 \leqslant \tau_1 \leqslant \tau_2$ (see the SM [72]). The joint WTD describes correlations between consecutive waiting times. When the waiting times are uncorrelated, the joint distribution factorizes as the product of two waiting time distributions [14], $\mathcal{W}_{\alpha\gamma\beta}^{\mathrm{unc}}(\tau_1, \tau_2) = \mathcal{W}_{\alpha\gamma}(\tau_1)\mathcal{W}_{\gamma\beta}(\tau_2)$. We can further quantify the correlations between consecutive waiting times using the correlation function

$$\delta\mathcal{W}_{\alpha\gamma\beta}(\tau_1, \tau_2) = \frac{\mathcal{W}_{\alpha\gamma\beta}(\tau_1, \tau_2) - \mathcal{W}_{\alpha\gamma}(\tau_1)\mathcal{W}_{\gamma\beta}(\tau_2)}{\mathcal{W}_{\alpha\gamma}(\tau_1)\mathcal{W}_{\gamma\beta}(\tau_2)}. \quad (4)$$

A main feature of the QSHI topological Andreev interferometer is that for an electron (say, spin-up) injected in NL, only (spin-down) holes and (spin-up) electrons can scatter into

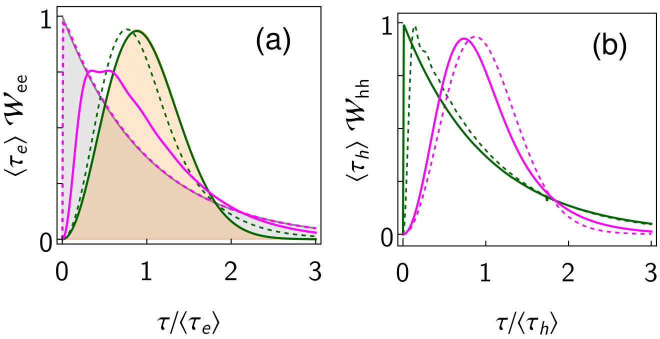

FIG. 2. Local WTDs, $\mathcal{W}_{ee}$ (a) and $\mathcal{W}_{hh}$ (b), for $L_S = 0.2$ (short junction, green) and $L_S = 1.5$ (long junction, magenta), with $\phi = 0$ for dashed lines and $\phi = \pi$ for solid ones. The gray (orange) shaded region indicate the Poisson (Wigner-Dyson) distribution.

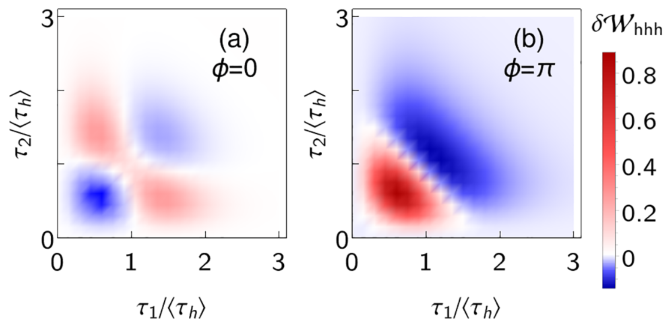

FIG. 3. Correlations between waiting times for three consecutive hole detections at NL, $\delta\mathcal{W}_{hhh}(\tau_1, \tau_2)$, for $L_S = 1.5$ as a function of τ_1 and τ_2 at (a) $\phi = 0$ and (b) $\phi = \pi$.

NL and NR, respectively. Thus, with electrons and holes always scattering into different leads, all local or same detector WTDs are necessarily given by $\mathcal{W}_{ee}$ and $\mathcal{W}_{hh}$, while all *nonlocal* WTDs are given by $\mathcal{W}_{eh}$ and $\mathcal{W}_{he}$, where measurements take place at different detectors. Similarly, $\mathcal{W}_{eee}$ and $\mathcal{W}_{hhh}$ are local joint WTDs, while joint distributions combining electron (NR) and hole (NL) measurements, like $\mathcal{W}_{ehe}$, are nonlocal.

Local waiting times. We start with the local WTDs $\mathcal{W}_{\alpha\alpha}$, representing two consecutive detections at either NL ($\alpha = h$) or NR ($\alpha = e$). It was established in Ref. [10] that the WTD of a quantum-coherent channel with energy-independent transmission is determined by its scattering probability: highly transmitting channels result in a Wigner-Dyson distribution [orange area in Fig. 2(a)], describing a coherent particle flow, while low-transmitting channels result in a Poisson distribution [gray area in Fig. 2(a)], characteristic of tunnel transport. In both cases, the impossibility of a simultaneous measurement of two particles at the same detector due to the Pauli exclusion principle forces the WTDs to be zero at $\tau = 0$. Owing to the constrained transport at the QSHI edge, with, e.g., $|\mathcal{S}_{hL,eL}|^2 + |\mathcal{S}_{eR,eL}|^2 = 1$, the transition between the Wigner-Dyson and Poisson distributions is here controlled by the length of the Andreev interferometer $2L_S$. Long (short) junctions [70] with $L_S > \xi$ ($L_S < \xi$) give a high probability of Andreev reflection $|\mathcal{S}_{hL,eL}|^2$ (electron transmission $|\mathcal{S}_{eR,eL}|^2$), and result in a Poisson (Wigner-Dyson) distribution (see the SM [72]). This behavior is consistent with earlier results [10,36,39], since the scattering probabilities for the topological Andreev interferometer are almost constant at subgap energies (see the SM [72]). As a result, any gapped state, at any phase ϕ, qualitatively follows the $\phi = 0$ local WTDs represented in Fig. 2 by dashed lines.

By contrast, for gapless MBSs around $\phi \sim \pi$ the low-energy electron transmission probability becomes strongly energy dependent for long junctions due to the resonant tunneling through the MBS [65] (also see the SM [72]). Consequently, we find that $\mathcal{W}_{ee}$ converges to the WTD of a resonant level in the tunnel limit [10], [solid magenta line in Fig. 2(a)], instead of evolving into a Poisson distribution like for $\phi = 0$. At high transmission (short junctions), the variation with the phase of $\mathcal{W}_{ee}$ is less noticeable [green lines in Fig. 2(a)]. This is also the case for the distribution of reflected holes $\mathcal{W}_{hh}$ at any transparency [Fig. 2(b)], since the probability of Andreev reflection is $|\mathcal{S}_{hL,eL}|^2 \sim 1$ for all the energies in the transport window ($|E| \leqslant eV$).

Even though $\mathcal{W}_{hh}$ is not very sensitive to the presence of the MBS, the correlations between consecutive waiting times for hole transfers $\delta\mathcal{W}_{hhh}$ contain very relevant information. We focus on long junctions, $L_S > \xi$, which are dominated by Andreev reflection processes and feature a more pronounced dependence on the phase ϕ. For gapful states ($\phi = 0$), the Andreev interferometer behaves like an electron-hole beam splitter, featuring the same correlations as a standard quantum point contact for electrons [14] [Fig. 3(a)]: When the time between two hole transfers is small, $\tau_1 < \langle\tau_h\rangle$ (or long, $\tau_1 > \langle\tau_h\rangle$), the next hole detection at τ_2 will require a long (short) waiting time (red color signals positive correlations). By contrast, gapless MBSs around $\phi \sim \pi$ exhibit correlations that seemingly explode at short waiting times, with values increasing an order of magnitude compared to the gapful case [Fig. 3(b)]. This means that short time intervals between detections are the most likely. The waiting times between electron transfers, on the other hand, are completely uncorrelated, i.e., $\delta\mathcal{W}_{eee}(\tau_1, \tau_2) \simeq \mathcal{W}_{ee}(\tau_1)\mathcal{W}_{ee}(\tau_2)$ (see the SM [72]).

Nonlocal waiting times. We now fully exploit the multiterminal advantage of the topological Andreev interferometer by exploring the nonlocal WTDs. By definition, the distribution $\mathcal{W}_{\alpha\beta}$, with $\beta \neq \alpha$, assumes that the first particle α has been detected; no matter how unlikely that event is. Therefore, the nonlocal waiting times are determined by the probability of the second detection. Consequently, $\mathcal{W}_{eh}$ ($\mathcal{W}_{he}$) is determined by the Andreev reflection (electron transmission) probability, following a behavior similar to $\mathcal{W}_{hh}$ ($\mathcal{W}_{ee}$), which we verify in Fig. 4. The one marked difference between local and nonlocal distributions is that, as particles transfer into different detectors, nonlocal WTDs can be finite at zero waiting time and also always fulfill $\mathcal{W}_{eh}(0) = \mathcal{W}_{he}(0)$ [36].

The nonlocal WTDs at zero waiting time have already been established to increase in the presence of MBSs, independently of the scattering probabilities [36]. Here, we interestingly also find that $\mathcal{W}_{he}(\tau)$, which for $\phi = \pi$ is determined by the Majorana-assisted electron tunneling, is further strongly altered. Specifically, $\mathcal{W}_{he}(\tau)$ presents a dip at short but finite waiting times. We explain this behavior as being due to the transition between a regime dominated by the Andreev reflection probability at $\tau \to 0$ into a regime where electron

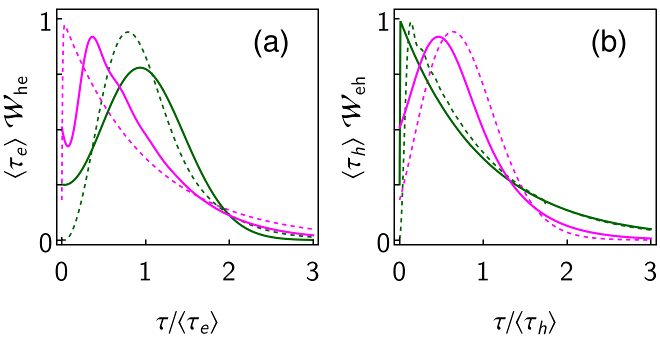

FIG. 4. Nonlocal WTDs, $\mathcal{W}_{he}$ (a) and $\mathcal{W}_{eh}$ (b), for $L_S = 0.2$ (short junction, green) and $L_S = 1.5$ (long junction, magenta), with $\phi = 0$ for dashed lines and $\phi = \pi$ for solid ones.

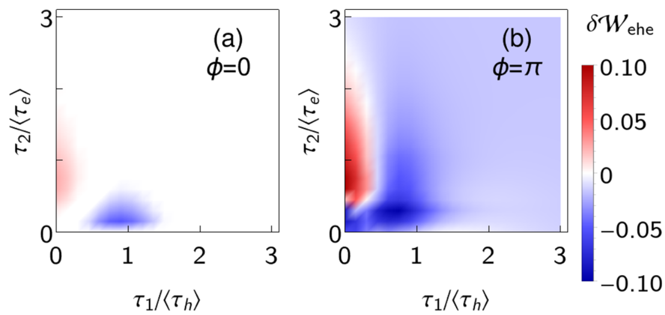

FIG. 5. Correlations between waiting times for the detection sequence electron-hole-electron between NL and NR: $\delta\mathcal{W}_{ehe}(\tau_1, \tau_2)$ for $L_S = 1.5$ as a function of τ_1 and τ_2 at (a) $\phi = 0$ and (b) $\phi = \pi$.

transmissions dominate at long waiting times. The former initially reduces the probability, while the latter imposes a behavior similar to the local distribution, $\mathcal{W}_{ee}$. The dip, or local minimum at short waiting times, reflects this transition and is particularly visible in the presence of Majorana-induced resonant tunneling when the corresponding local WTD becomes anomalous, see Fig. 2(a). With $\mathcal{W}_{eh}$ being primarily determined by $\mathcal{W}_{hh}$, we find no such dip in $\mathcal{W}_{eh}$. This behavior of $\mathcal{W}_{he}$ is unique to the topological Andreev interferometer, which we confirmed by checking both local and nonlocal WTDs for an ordinary interferometer, in the absence of any topology.

We further find that the correlations between nonlocal waiting times also show a unique dependence on the phase ϕ. We focus on alternate electron-hole-electron transfers in the long junction regime, where the phase dependence is stronger, and study the behavior of $\mathcal{W}_{ehe}$ containing the correlations between $\mathcal{W}_{he}$ and $\mathcal{W}_{eh}$. Very short waiting times, $\tau_1 < \langle\tau_h\rangle$, show only a weak correlation with long waiting times ($\tau_2 > \langle\tau_e\rangle$) for gapful states ($\phi = 0$), but this behavior is enhanced two orders of magnitude for gapless MBS around $\phi \sim \pi$ (Fig. 5). As mentioned above, the sequential tunneling of three electrons $\mathcal{W}_{eee}$ is uncorrelated. However, including one hole detection between the electron transfers drastically changes the statistics in the presence of MBSs. These results indicate that to completely characterize gapless states in Andreev interferometers, we need to compare transport processes in both arms of the circuit. We note that $\mathcal{W}_{heh}$, which is dominated by Andreev reflections and thus less sensitive to the presence of the SL-SR junction, shows negative correlations and a weak phase dependence (see the SM [72]). The behavior of all studied WTDs and correlations is summarized in Table I.

Concluding remarks. We have analyzed the distribution of waiting times and their correlations for electrons and holes emitted from a topological Andreev interferometer: a NL-SL-SR-NR junction on the quantum spin Hall edge. Two special features of this setup are (i) the emergence of gapless MBSs and (ii) it acting as an electron-hole beam splitter, sending holes and electrons to different leads. This topological Andreev interferometer is thus one of the simplest multiterminal setups without magnetic elements that features MBSs and allows us to test their nonlocal behavior. We find that the gapless property of the MBSs makes the waiting times involving Majorana-assisted electron transfers, $\mathcal{W}_{ee}$ and $\mathcal{W}_{he}$, very special around $\phi \sim \pi$. Most importantly, the nonlocal property of MBSs is captured in the correlations between waiting times, see Table I. For example, the waiting times for consecutive hole reflections and for alternate electron-hole detections are strongly correlated for gapless Majorana states [Fig. 3(b) and Fig. 5(b)], even if their distributions, $\mathcal{W}_{hh}$ and $\mathcal{W}_{eh}$, are almost insensitive to the phase ϕ.

The search for signatures of Majorana states currently faces several challenges [30,31,73–75]. In particular, the presence of trivial low-energy modes that mimic the local properties of MBSs, obscuring their detection in many platforms. To circumvent the latter, the quantum spin Hall effect is a promising platform where signatures of gapless MBSs have already been identified experimentally, even in the presence of extra trivial modes [51–53]. Thus, Andreev reflection and normal transmissions, which determine all our results, are the dominant scattering processes. Furthermore, our analysis of nonlocal properties of Majorana states addresses the need to go beyond local signatures. In fact, previous studies have already analyzed the WTD of electrons tunneling into a Majorana state [35,36,38,39] focusing on its local properties and showing that the resonant transport through a MBS yields WTDs very similar to that of a single (trivial) level resonance [10,36]. Therefore, our results complement earlier work by showing that taking into account independent and simultaneous transfers of electrons and holes into separate detectors (i.e., both local and nonlocal WTDs), and the correlations between them, yields distinctive signatures of Majorana modes. Also, despite

TABLE I. Summary of the behaviors of WTDs and joint WTDs for $L_S > \xi$. Here, WD and P indicate, respectively, Wigner-Dyson and Poisson distributions.

WTD	$\phi = 0$	$\phi = \pi$
$\mathcal{W}_{ee}$	P	Resonant level
$\mathcal{W}_{hh}$	WD	WD
$\mathcal{W}_{eh}$	$\mathcal{W}_{eh}(0) \approx 0$, WD	$\mathcal{W}_{eh}(0) > 0$, WD
$\mathcal{W}_{he}$	$\mathcal{W}_{he}(0) \approx 0$, P	$\mathcal{W}_{he}(0) > 0$, P with dip
$\delta\mathcal{W}_{eee}$	Uncorrelated	Uncorrelated
$\delta\mathcal{W}_{hhh}$	Bream splitter	$\delta\mathcal{W}_{hhh} \sim 1$ at $\tau_{1,2} < \langle\tau_h\rangle$
$\delta\mathcal{W}_{heh}$	Low correlation	Low correlation
$\delta\mathcal{W}_{ehe}$	Low correlation	$\delta\mathcal{W}_{ehe} \sim 0.1$ at $\tau_1 < \langle\tau_h\rangle$

the challenges involved in measuring waiting times, there are promising new advances like experimental measurements of time-of-flight of electron excitations [76,77], in addition to recent theoretical proposals for WTD clocks [78,79].

Acknowledgments. Work done at PRL is supported by Department of Space, Government of India. P.D. thanks D. Chakraborty, P. Holmvall, and I. Mahyaeh for technical help, U. Basu for discussions, and acknowledges the computational facilities by Uppsala University and the Department of Science and Technology (DST), India, for the financial support through SERB Start-up Research Grant (File No. SRG/2022/001121). J.C. acknowledges financial support from the Swedish Research Council (Vetenskapsrådet Grant No. 2021-04121), the Scandinavia-Japan Sasakawa Foundation (Grant No. GA22-SWE-0028), the Royal Swedish Academy of Sciences (Grant No. PH2022-0003), and the Carl Trygger's Foundation (Grant No. 22: 2093). A.B.S. acknowledges financial support from the Knut and Alice Wallenberg Foundation through the Wallenberg Academy Fellows program and the EU-COST Action CA-21144 Superqumap. P.B. acknowledges support from the Spanish CM "Talento Program" Project No. 2019-T1/IND-14088 and the Agencia Estatal de Investigación Projects No. PID2020-117992GA-I00 and No. CNS2022-135950.

[1] Y. M. Blanter and M. Büttiker, Shot noise in mesoscopic conductors, Phys. Rep. **336**, 1 (2000).

[2] L. S. Levitov, H. Lee, and G. B. Lesovik, Electron counting statistics and coherent states of electric current, J. Math. Phys. **37**, 4845 (1996).

[3] D. A. Bagrets and Y. V. Nazarov, Full counting statistics of charge transfer in Coulomb blockade systems, Phys. Rev. B **67**, 085316 (2003).

[4] D. A. Bagrets, Y. Utsumi, D. S. Golubev, and G. Schön, Full counting statistics of interacting electrons, Fortschr. Phys. **54**, 917 (2006).

[5] N. Camus, E. Yakaboylu, L. Fechner, M. Klaiber, M. Laux, Y. Mi, K. Z. Hatsagortsyan, T. Pfeifer, C. H. Keitel, and R. Moshammer, Experimental evidence for quantum tunneling time, Phys. Rev. Lett. **119**, 023201 (2017).

[6] A. Kurzmann, P. Stegmann, J. Kerski, R. Schott, A. Ludwig, A. D. Wieck, J. König, A. Lorke, and M. Geller, Optical detection of single-electron tunneling into a semiconductor quantum dot, Phys. Rev. Lett. **122**, 247403 (2019).

[7] S. Singh, P. Menczel, D. S. Golubev, I. M. Khaymovich, J. T. Peltonen, C. Flindt, K. Saito, É. Roldán, and J. P. Pekola, Universal first-passage-time distribution of non-Gaussian currents, Phys. Rev. Lett. **122**, 230602 (2019).

[8] M. Albert, C. Flindt, and M. Büttiker, Distributions of waiting times of dynamic single-electron emitters, Phys. Rev. Lett. **107**, 086805 (2011).

[9] M. Albert, G. Haack, C. Flindt, and M. Büttiker, Electron waiting times in mesoscopic conductors, Phys. Rev. Lett. **108**, 186806 (2012).

[10] G. Haack, M. Albert, and C. Flindt, Distributions of electron waiting times in quantum-coherent conductors, Phys. Rev. B **90**, 205429 (2014).

[11] G.-M. Tang, F. Xu, and J. Wang, Waiting time distribution of quantum electronic transport in the transient regime, Phys. Rev. B **89**, 205310 (2014).

[12] K. H. Thomas and C. Flindt, Waiting time distributions of noninteracting fermions on a tight-binding chain, Phys. Rev. B **89**, 245420 (2014).

[13] B. Sothmann, Electronic waiting-time distribution of a quantum-dot spin valve, Phys. Rev. B **90**, 155315 (2014).

[14] D. Dasenbrook, P. P. Hofer, and C. Flindt, Electron waiting times in coherent conductors are correlated, Phys. Rev. B **91**, 195420 (2015).

[15] P. Burset, J. Kotilahti, M. Moskalets, and C. Flindt, Time-domain spectroscopy of mesoscopic conductors using voltage pulses, Adv. Quantum Technol. **2**, 1900014 (2019).

[16] S. L. Rudge and D. S. Kosov, Nonrenewal statistics in quantum transport from the perspective of first-passage and waiting time distributions, Phys. Rev. B **99**, 115426 (2019).

[17] N. S. Davis, S. L. Rudge, and D. S. Kosov, Electronic statistics on demand: Bunching, antibunching, positive, and negative correlations in a molecular spin valve, Phys. Rev. B **103**, 205408 (2021).

[18] S. K. Gorman, Y. He, M. G. House, J. G. Keizer, D. Keith, L. Fricke, S. J. Hile, M. A. Broome, and M. Y. Simmons, Tunneling statistics for analysis of spin-readout fidelity, Phys. Rev. Appl. **8**, 034019 (2017).

[19] S. Matsuo, K. Kuroyama, S. Yabunaka, S. R. Valentin, A. Ludwig, A. D. Wieck, and S. Tarucha, Full counting statistics of spin-flip and spin-conserving charge transitions in Pauli-spin blockade, Phys. Rev. Res. **2**, 033120 (2020).

[20] F. Brange, A. Schmidt, J. C. Bayer, T. Wagner, C. Flindt, and R. J. Haug, Controlled emission time statistics of a dynamic single-electron transistor, Sci. Adv. **7**, eabe0793 (2021).

[21] M. Jenei, E. Potanina, R. Zhao, K. Y. Tan, A. Rossi, T. Tanttu, K. W. Chan, V. Sevriuk, M. Möttönen, and A. Dzurak, Waiting time distributions in a two-level fluctuator coupled to a superconducting charge detector, Phys. Rev. Res. **1**, 033163 (2019).

[22] A. Ranni, F. Brange, E. T. Mannila, C. Flindt, and V. F. Maisi, Real-time observation of Cooper pair splitting showing strong non-local correlations, Nat. Commun. **12**, 6358 (2021).

[23] C. L. Kane and E. J. Mele, Quantum spin Hall effect in graphene, Phys. Rev. Lett. **95**, 226801 (2005).

[24] L. Fu and C. L. Kane, Superconducting proximity effect and Majorana fermions at the surface of a topological insulator, Phys. Rev. Lett. **100**, 096407 (2008).

[25] L. Fu and C. L. Kane, Josephson current and noise at a superconductor/quantum-spin-Hall-insulator/superconductor junction, Phys. Rev. B **79**, 161408(R) (2009).

[26] X.-L. Qi and S.-C. Zhang, Topological insulators and superconductors, Rev. Mod. Phys. **83**, 1057 (2011).

[27] V. Mourik, K. Zuo, S. M. Frolov, S. R. Plissard, E. P. A. Bakkers, and L. P. Kouwenhoven, Signatures of Majorana fermions in hybrid superconductor-semiconductor nanowire devices, Science **336**, 1003 (2012).

[28] A. P. Higginbotham, S. M. Albrecht, G. Kirsanskas, W. Chang, F. Kuemmeth, P. Krogstrup, T. S. Jespersen, J. Nygård, K. Flensberg, and C. M. Marcus, Parity lifetime of bound states in a proximitized semiconductor nanowire, Nat. Phys. **11**, 1017 (2015).

[29] M. T. Deng, S. Vaitiekėnas, E. B. Hansen, J. Danon, M. Leijnse, K. Flensberg, J. Nygård, P. Krogstrup, and C. M. Marcus, Majorana bound state in a coupled quantum-dot hybrid-nanowire system, Science **354**, 1557 (2016).

[30] J. Chen, B. D. Woods, P. Yu, M. Hocevar, D. Car, S. R. Plissard, E. P. A. M. Bakkers, T. D. Stanescu, and S. M. Frolov, Ubiquitous non-Majorana zero-bias conductance peaks in nanowire devices, Phys. Rev. Lett. **123**, 107703 (2019).

[31] P. Yu, J. Chen, M. Gomanko, G. Badawy, E. P. A. M. Bakkers, K. Zuo, V. Mourik, and S. M. Frolov, Non-Majorana states yield nearly quantized conductance in proximatized nanowires, Nat. Phys. **17**, 482 (2021).

[32] L. Rajabi, C. Pöltl, and M. Governale, Waiting time distributions for the transport through a quantum-dot tunnel coupled to one normal and one superconducting lead, Phys. Rev. Lett. **111**, 067002 (2013).

[33] M. Albert, D. Chevallier, and P. Devillard, Waiting times of entangled electrons in normal–superconducting junctions, Physica E **76**, 209 (2016).

[34] N. Walldorf, C. Padurariu, A.-P. Jauho, and C. Flindt, Electron waiting times of a Cooper pair splitter, Phys. Rev. Lett. **120**, 087701 (2018).

[35] D. Chevallier, M. Albert, and P. Devillard, Probing Majorana and Andreev bound states with waiting times, Europhys. Lett. **116**, 27005 (2016).

[36] S. Mi, P. Burset, and C. Flindt, Electron waiting times in hybrid junctions with topological superconductors, Sci. Rep. **8**, 16828 (2018).

[37] K. Wrześniewski and I. Weymann, Current cross-correlations and waiting time distributions in Andreev transport through Cooper pair splitters based on a triple quantum dot system, Phys. Rev. B **101**, 155409 (2020).

[38] W. Fu, S.-S. Ke, Y. Guo, H.-W. Zhang, and H.-F. Lü, Waiting time distribution and current correlations via a Majorana single-charge transistor, Phys. Rev. B **106**, 075404 (2022).

[39] F. Schulz, D. Chevallier, and M. Albert, Waiting time distributions in quantum spin Hall based heterostructures, Phys. Rev. B **107**, 245406 (2023).

[40] M. König, S. Wiedmann, C. Brüne, A. Roth, H. Buhmann, L. W. Molenkamp, X.-L. Qi, and S.-C. Zhang, Quantum spin Hall insulator state in HgTe quantum wells, Science **318**, 766 (2007).

[41] C. Brüne, A. Roth, E. G. Novik, M. Konig, H. Buhmann, E. M. Hankiewicz, W. Hanke, J. Sinova, and L. W. Molenkamp, Evidence for the ballistic intrinsic spin Hall effect in HgTe nanostructures, Nat. Phys. **6**, 448 (2010).

[42] I. Knez, R.-R. Du, and G. Sullivan, Evidence for helical edge modes in inverted InAs/GaSb quantum wells, Phys. Rev. Lett. **107**, 136603 (2011).

[43] C. Brüne, A. Roth, H. Buhmann, E. M. Hankiewicz, L. W. Molenkamp, J. Maciejko, X.-L. Qi, and S.-C. Zhang, Spin polarization of the quantum spin Hall edge states, Nat. Phys. **8**, 485 (2012).

[44] F. Reis, G. Li, L. Dudy, M. Bauernfeind, S. Glass, W. Hanke, R. Thomale, J. Schäfer, and R. Claessen, Bismuthene on a SiC substrate: A candidate for a high-temperature quantum spin Hall material, Science **357**, 287 (2017).

[45] J. Kammhuber, M. C. Cassidy, F. Pei, M. P. Nowak, A. Vuik, Ö. Gül, D. Car, S. R. Plissard, E. P. A. M. Bakkers, M. Wimmer, and L. P. Kouwenhoven, Conductance through a helical state in an Indium antimonide nanowire, Nat. Commun. **8**, 478 (2017).

[46] S. Wu, V. Fatemi, Q.-D. Gibson, K. Watanabe, T. Taniguchi, R.-J. Cava, and P. Jarillo-Herrero, Observation of the quantum spin Hall effect up to 100 Kelvin in a monolayer, Science **359**, 76 (2018).

[47] C. Wu, B. A. Bernevig, and S.-C. Zhang, Helical liquid and the edge of quantum spin Hall systems, Phys. Rev. Lett. **96**, 106401 (2006).

[48] C. Xu and J. E. Moore, Stability of the quantum spin Hall effect: Effects of interactions, disorder, and $\mathbb{Z}_2$ topology, Phys. Rev. B **73**, 045322 (2006).

[49] I. Knez, R.-R. Du, and G. Sullivan, Andreev reflection of helical edge modes in InAs/GaSb quantum spin Hall insulator, Phys. Rev. Lett. **109**, 186603 (2012).

[50] S. Hart, H. Ren, T. Wagner, P. Leubner, M. Mühlbauer, C. Brüne, H. Buhmann, L. W. Molenkamp, and A. Yacoby, Induced superconductivity in the quantum spin Hall edge, Nat. Phys. **10**, 638 (2014).

[51] J. Wiedenmann, E. Bocquillon, R. S. Deacon, S. Hartinger, O. Herrmann, T. M. Klapwijk, L. Maier, C. Ames, C. Brüne, C. Gould *et al.*, 4π-periodic Josephson supercurrent in HgTe-based topological Josephson junctions, Nat. Commun. **7**, 10303 (2016).

[52] E. Bocquillon, R. S. Deacon, J. Wiedenmann, P. Leubner, T. M. Klapwijk, C. Brüne, K. Ishibashi, H. Buhmann, and L. W. Molenkamp, Gapless Andreev bound states in the quantum spin Hall insulator HgTe, Nat. Nanotechnol. **12**, 137 (2017).

[53] R. S. Deacon, J. Wiedenmann, E. Bocquillon, F. Domínguez, T. M. Klapwijk, P. Leubner, C. Brüne, E. M. Hankiewicz, S. Tarucha, K. Ishibashi, H. Buhmann, and L. W. Molenkamp, Josephson radiation from gapless Andreev bound states in HgTe-based topological junctions, Phys. Rev. X **7**, 021011 (2017).

[54] S. Hart, H. Ren, M. Kosowsky, G. Ben-Shach, P. Leubner, C. Brüne, H. Buhmann, L. W. Molenkamp, B. I. Halperin, and A. Yacoby, Controlled finite momentum pairing and spatially varying order parameter in proximitized HgTe quantum wells, Nat. Phys. **13**, 87 (2017).

[55] E. Sajadi, T. Palomaki, Z. Fei, W. Zhao, P. Bement, C. Olsen, S. Luescher, X. Xu, J. A. Folk, and D. H. Cobden, Gate-induced superconductivity in a monolayer topological insulator, Science **362**, 922 (2018).

[56] V. Fatemi, S. Wu, Y. Cao, L. Bretheau, Q. D. Gibson, K. Watanabe, T. Taniguchi, R. J. Cava, and P. Jarillo-Herrero, Electrically tunable low-density superconductivity in a monolayer topological insulator, Science **362**, 926 (2018).

[57] P. Adroguer, C. Grenier, D. Carpentier, J. Cayssol, P. Degiovanni, and E. Orignac, Probing the helical edge states of a topological insulator by Cooper-pair injection, Phys. Rev. B **82**, 081303(R) (2010).

[58] A. M. Black-Schaffer and A. V. Balatsky, Odd-frequency superconducting pairing in topological insulators, Phys. Rev. B **86**, 144506 (2012).

[59] A. M. Black-Schaffer and A. V. Balatsky, Proximity-induced unconventional superconductivity in topological insulators, Phys. Rev. B **87**, 220506(R) (2013).

[60] F. Crépin, P. Burset, and B. Trauzettel, Odd-frequency triplet superconductivity at the helical edge of a topological insulator, Phys. Rev. B **92**, 100507(R) (2015).

[61] G. Tkachov, P. Burset, B. Trauzettel, and E. M. Hankiewicz, Quantum interference of edge supercurrents in a two-dimensional topological insulator, Phys. Rev. B **92**, 045408 (2015).

[62] J. Cayao and A. M. Black-Schaffer, Odd-frequency superconducting pairing and subgap density of states at the edge of a two-dimensional topological insulator without magnetism, Phys. Rev. B **96**, 155426 (2017).

[63] F. Keidel, P. Burset, and B. Trauzettel, Tunable hybridization of Majorana bound states at the quantum spin Hall edge, Phys. Rev. B **97**, 075408 (2018).

[64] F. Keidel, S.-Y. Hwang, B. Trauzettel, B. Sothmann, and P. Burset, On-demand thermoelectric generation of equal-spin Cooper pairs, Phys. Rev. Res. **2**, 022019(R) (2020).

[65] J. Cayao, P. Dutta, P. Burset, and A. M. Black-Schaffer, Phase-tunable electron transport assisted by odd-frequency Cooper pairs in topological Josephson junctions, Phys. Rev. B **106**, L100502 (2022).

[66] B. Lu, G. Cheng, P. Burset, and Y. Tanaka, Identifying Majorana bound states at quantum spin Hall edges using a metallic probe, Phys. Rev. B **106**, 245427 (2022).

[67] J. Eom, C.-J. Chien, and V. Chandrasekhar, Phase dependent thermopower in Andreev interferometers, Phys. Rev. Lett. **81**, 437 (1998).

[68] D. A. Dikin, S. Jung, and V. Chandrasekhar, Low-temperature thermal properties of mesoscopic normal-metal/superconductor heterostructures, Phys. Rev. B **65**, 012511 (2001).

[69] A finite separation of the SL and SR arms, or asymmetry in the superconductor lengths, would not qualitatively affect our results.

[70] Superconductor-normal metal-superconductor junctions with the normal intermediate region much smaller than the superconducting coherence length are usually referred to as *short* junctions. We work in this regime, but use the terms *short* and *long* junctions to distinguish the cases where the total size of the SL-SR segment ($2L_S$) is smaller or larger, respectively, than the superconducting coherence length ξ.

[71] Our results are mostly insensitive to the chemical potential and do not qualitatively change for voltages within the gap.

[72] See Supplemental Material at http://link.aps.org/supplemental/10.1103/PhysRevResearch.6.L012062 for details of the theoretical formalism and some additional results to support the discussions of the main text about the scattering probabilities, the bias dependence of the waiting time distributions, and the nonlocal joint waiting time correlations.

[73] E. Prada, P. San-Jose, M. W. A. de Moor, A. Geresdi, E. J. H. Lee, J. Klinovaja, D. Loss, J. Nygård, R. Aguado, and L. P. Kouwenhoven, From Andreev to Majorana bound states in hybrid superconductor–semiconductor nanowires, Nat. Rev. Phys. **2**, 575 (2020).

[74] E. Kleinherbers, A. Schünemann, and J. König, Full counting statistics in a Majorana single-charge transistor, Phys. Rev. B **107**, 195407 (2023).

[75] R. A. Dourado, P. H. Penteado, and J. C. Egues, Nonlocality of local Andreev conductances as a probe for topological Majorana wires, arXiv:2303.01867.

[76] M. Kataoka, N. Johnson, C. Emary, P. See, J. P. Griffiths, G. A. C. Jones, I. Farrer, D. A. Ritchie, M. Pepper, and T. J. B. M. Janssen, Time-of-flight measurements of single-electron wave packets in quantum Hall edge states, Phys. Rev. Lett. **116**, 126803 (2016).

[77] G. Roussely, E. Arrighi, G. Georgiou, S. Takada, M. Schalk, M. Urdampilleta, A. Ludwig, A. D. Wieck, P. Armagnat, T. Kloss *et al.*, Unveiling the bosonic nature of an ultrashort few-electron pulse, Nat. Commun. **9**, 2811 (2018).

[78] G. Haack, A. Steffens, J. Eisert, and R. Hübener, Continuous matrix product state tomography of quantum transport experiments, New J. Phys. **17**, 113024 (2015).

[79] D. Dasenbrook and C. Flindt, Quantum theory of an electron waiting time clock, Phys. Rev. B **93**, 245409 (2016).